

Short Article

Megakaryocyte and arteriolar niches regulate distinct lineage-biased hematopoietic stem cells

Sandra Pinho^{1,2,3}, Tony Marchand^{1,2,4}, Sten Eirik W. Jacobsen^{5,6}, Claus Nerlov⁷ and Paul S. Frenette^{1,2,3,8}

¹Ruth L. and David S. Gottesman Institute for Stem Cell and Regenerative Medicine Research,

²Department of Cell Biology,

³Department of Medicine, Albert Einstein College of Medicine, Bronx, NY 10461, USA

⁴INSERM U1236, Université Rennes 1, Rennes, France

⁵Department of Cell and Molecular Biology, Wallenberg Institute for Regenerative Medicine,

⁶Department of Medicine Huddinge, Center for Hematology and Regenerative Medicine, Karolinska Institutet, Stockholm, Sweden

⁷MRC Molecular Haematology Unit, Weatherall Institute of Molecular Medicine, University of Oxford, Oxford, UK

⁸Lead contact

Correspondence:

Paul S. Frenette

paul.frenette@einstein.yu.edu

Albert Einstein College of Medicine

Michael F. Price Center

1301 Morris Park Avenue, Room 101

Bronx, NY 10461

Tel: 718.678.1255

Fax: 718.678.1018

SUMMARY

The spatial localization of hematopoietic stem cells (HSCs) in the bone marrow (BM) remains controversial with studies suggesting that they are maintained in homogenously distributed niches while others have suggested the contributions of distinct niche structures. Subsets of quiescent HSCs have indeed been reported to associate with megakaryocytes (MK) or arterioles in the BM. However, these HSC subsets have not been prospectively defined. Here, we show that platelet and myeloid-biased HSCs, marked by von Willebrand factor (vWF) expression, are highly enriched in MK niches. Depletion of MK selectively expands vWF⁺ HSCs whereas the depletion of NG2⁺ arteriolar niche cells selectively depletes vWF⁻ HSCs. In addition, MK depletion eliminates lineage bias and confers balanced hematopoietic cell production by vWF⁺ HSCs after transplantation. These studies thus suggest the existence of at least two spatially and functionally distinct bone marrow niches for HSC subsets with distinct developmental potential.

KEYWORDS

HSC; lineage-biased HSCs; von Willebrand factor; niche; megakaryocyte niche; arteriolar niche

INTRODUCTION

Despite intense investigation, there remains controversy about the precise location of hematopoietic stem cells (HSCs) in the bone marrow (BM). Initial studies have suggested a close relationship with osteoblasts in the endosteal region (Zhang et al., 2003). Subsequent studies, with the advent of SLAM markers, have shown that CD150⁺ CD48⁻ Lineage⁻ CD41⁻ HSCs were distributed broadly in close proximity of endothelial and Nestin-GFP⁺ perivascular cells (Kiel et al., 2005; Mendez-Ferrer et al., 2010). Further improvement in imaging technologies allowing tridimensional (3D) visualization of endogenous HSCs in the BM have uncovered heterogeneity among Nestin-GFP⁺ cells with a subset of quiescent HSCs showing a significant association with Nestin-GFP-bright arteriole structures (Kunisaki et al., 2013). Upon deletion of periarteriolar NG2⁺ stromal cells or after inducing HSC proliferation, HSCs were shown to redistribute away from arteriole structures (Kunisaki et al., 2013). Further studies show that in a spatially distinct niche from the arteriolar one, another subset of HSCs exhibit a significant association with megakaryocytes (MK) (Bruns et al., 2014). Selective deletion of MK induced HSC proliferation in a manner shown to depend on CXCL4 (also called platelet factor-4, PF4), TGF- β or thrombopoietin production by MK (Bruns et al., 2014; Nakamura-Ishizu et al., 2014; Zhao et al., 2014). These studies thus suggest that both arteriole structures and MK are niche sites promoting HSC quiescence. However, other studies using α -catulin⁺ c-Kit⁺ Lineage⁻ to mark HSCs have shown in cleared BM that these HSCs were uniformly distributed near sinusoids in a manner indistinguishable from randomly placed dots (Acar et al., 2015). Other analyses, in support of multiple niche structures, have also suggested the existence of distinct arteriolar and MK niche harboring reactive oxygen species (ROS)-low quiescent HSCs (Itkin et

al., 2016), or HSC association with type H endothelial cells bridging arterioles and sinusoids in developing bones (Kusumbe et al., 2016). As sinusoids are evenly distributed throughout the BM (Kunisaki et al., 2013), every hematopoietic cell is expected to be relatively close to them (~15 μ m on average), raising questions on the niche specificity. Indeed, the relationship of HSCs with sinusoid vessels was not found to be significantly different from computational modeling random dots (Acar et al., 2015; Kunisaki et al., 2013). However, one study, using a *Hoxb5* reporter, found that these HSCs significantly associated with sinusoidal endothelial cells in the BM (Chen et al., 2016). Thus, these studies using different HSC markers have reported differing results about HSC localization in the BM.

HSCs are known to be functionally heterogeneous (Copley et al., 2012; Muller-Sieburg et al., 2012). For example, transplantation of single HSCs has revealed reproducible bias toward selective differentiation to the myeloid or the lymphoid lineage (Dykstra et al., 2007). Using von Willebrand factor (vWF) promoter to drive GFP in transgenic mice (*Vwf-eGFP*), GFP was shown to mark a subset of quiescent HSCs that exhibit platelet and myeloid bias upon transplantation whereas the GFP⁻ HSC subset was lymphoid biased (Sanjuan-Pla et al., 2013). Expression of CD41 (Gekas and Graf, 2013) or c-Kit (Shin et al., 2014) have also been suggested to mark a megakaryocytic-biased HSC subset. Here, we show that myeloid and lymphoid-biased HSCs occupy distinct niches microenvironment that are differentially regulated in the BM.

RESULTS AND DISCUSSION

vWF⁺ HSCs associate with megakaryocytes, but not arterioles, in the mouse bone marrow

We evaluated the relationships of platelet- and myeloid-biased vWF-eGFP⁺ and

lymphoid-biased vWF -eGFP⁻ HSCs (henceforth designated vWF ⁺ and vWF ⁻ HSCs) with MK and arteriolar niches in *Vwf-eGFP* mice. We prepared whole-mount sternal BM of *Vwf-eGFP* mice to image by 3D confocal immunofluorescence analyses where HSCs are identified with Lineage⁻ CD48⁻ CD150⁺ and where GFP marks both MK and a subset of HSCs in BM (Asada et al., 2017; Bruns et al., 2014; Kunisaki et al., 2013) (**Figure 1A and 1B**). vWF ⁺ HSCs constitute a rare fraction of the Lineage⁻ Sca1⁺ c-Kit⁺ (LSK) CD48⁻ CD150⁺ HSC population ($24.0 \pm 1.4\%$, mean \pm S.E.M.), as measured by FACS analysis (**Figure S1A**). However, $77.2 \pm 9.9\%$ of vWF ⁺ HSCs were located within 5 μ m distance from MK (**Figure 1B, 1C and S1B**), with a considerable fraction ($70.8 \pm 17.2\%$) laying directly adjacent to MKs (**Figure 1E**), which is significantly different from random association. By contrast to vWF ⁻ HSCs, vWF ⁺ HSCs did not show any significant association with arterioles (identified by morphology and intravenous injection of CD31 in combination with CD144 or by Sca1^{high} staining) in the mouse BM and their distribution was statistically different from that of lymphoid-biased HSCs relative to arterioles (**Figure 1B, 1D, 1E and S1C**). These data suggest that the existence of at least two spatially distinct BM niches for subsets of HSCs with distinct developmental potential.

vWF ⁺, but not vWF ⁻, HSC proliferation is regulated by megakaryocytes

To investigate the role of MK *in vivo* in these lineage-biased HSC regulation, we generated *Cxcl4-cre;iDTR;Vwf-eGFP* mice. Control *iDTR;Vwf-eGFP* and triple transgenic *Cxcl4-cre;iDTR;Vwf-eGFP* mice were treated with diphtheria toxin (DT) (**Figure 2A**) to deplete MK as previously described (Bruns et al., 2014). Seven days after the initial dose, we evaluated the impact on HSC numbers. As previously reported (Bruns et al., 2014), MK depletion significantly increased the number of phenotypic HSCs in BM. Strikingly, we found that MK

depletion selectively increased (by 11.4-fold, $p < 0.0001$) the number of vWF^+ HSCs whereas the number of vWF^- HSCs modestly expanded 1.4-fold (**Figure 2B-E**). Evaluation of the bone marrow 3D distribution of vWF^- and vWF^+ HSCs in steady-state and MK-depleted mice revealed no significant alterations in their relationships with arterioles (**Figure S2**). These data thus suggest that MK specifically regulate the vWF^+ subset of HSCs.

vWF^+ HSC reconstitution potential is regulated by megakaryocytes

We next evaluated the impact of MK depletion on the ability of vWF^- and vWF^+ HSCs obtained from steady-state and MK-depleted mice to reconstitute hematopoietic lineages after transplantation (**Figure S3A**). Competitive transplantation of sorted LSK $CD48^- CD150^+ vWF^-$ and vWF^+ HSCs revealed that vWF^+ HSCs exhibited a biased toward repopulation of platelets (**Figures 2F, S3B and S3C**) and myeloid cells (**Figure 2G and S3C**) compared to vWF^- HSCs, as previously shown (Sanjuan-Pla et al., 2013). The capacity to generate platelets and myeloid cells was preserved after MK depletion (**Figure 2F and S3C**). In fact, HSCs were more balanced in their lineage generation upon MK depletion (**Figure 2G and S3C**), suggesting the interesting possibility that MK can further regulate HSC fate. While the overall long-term engraftment of vWF^- and vWF^+ HSCs was not statistically different after MK depletion (**Figure 2H**), the repopulation capacity of HSCs from MK-depleted mice was reduced (**Figure 2H**, note the y axis values), likely due to proliferation as previously noted (Bruns et al., 2014; Passegue et al., 2005).

In addition, analysis of the BM 16 weeks after transplantation revealed that whereas both HSC subsets from MK-depleted mice were capable to reconstitute the $CD45.2^+ LSK CD48^- CD150^+ vWF^-$ HSC compartment (**Figure S3D**, right plots), the ability of vWF^+ HSCs to reconstitute $CD45.2^+ LSK CD48^- CD150^+ vWF^+$ HSCs was compromised (**Figure S3D**). We

found that donor vWF^- HSCs, harvested from either steady-state or MK-depleted mice, were not able to regenerate the vWF^+ HSC compartment (**Figure S3D**), which is consistent with previous analyses (Sanjuan-Pla et al., 2013). These results suggest that MK selectively regulate the proliferation and fate of the vWF^+ HSC subset.

NG2⁺ arteriolar niche cells selectively regulate vWF^- lymphoid-biased HSC quiescence and distribution in bone marrow

NG2⁺ periarteriolar cell depletion leads to an altered localization of the HSC subset associated with arterioles and increases the proportion of proliferative HSCs (Kunisaki et al., 2013). To investigate the impact of arteriolar niche depletion on the vWF^+ and vWF^- HSC subsets, we generated *NG2-cre^{ERTM};iDTR;Vwf-eGFP* mice. Triple transgenic *NG2-cre^{ERTM};iDTR;Vwf-eGFP* and control *iDTR;Vwf-eGFP* mice were treated with tamoxifen and DT to induce NG2⁺ cell depletion, and analyzed 16 days later by FACS and whole-mount immunofluorescence imaging of the sternal BM (**Figure 3A**). We found that NG2⁺ cells depletion led to significant (~50%) reductions in the number of phenotypic LSK CD48⁻ CD150⁺ lymphoid-biased vWF^- HSCs compared to control *iDTR* mice (**Figure 3B-E**). By contrast to MK depletion, vWF^+ HSC numbers were not significantly affected by NG2⁺ cells depletion and disruption of the arteriolar niche (**Figure 3B-E**). We next evaluated the relationships of HSCs with MK and arterioles by 3D imaging. Interestingly, while NG2⁺ cell depletion did not affect the relationship of remaining vWF^- (**Figure 4A** or vWF^+ HSCs (**Figure 4B**) with MK, it selectively altered vWF^- HSC localization relative to arterioles (**Figure 4C**; $P < 0.0001$), but not that of vWF^+ HSCs (**Figure 4D**). These results suggest that MK and arterioles regulate distinct HSC subsets in the BM.

Finally, we examined the reconstitution potential of sorted vWF^{-} and vWF^{+} HSCs harvested from $NG2^{+}$ depleted and control animals (**Figure S4A**). Peripheral blood lineage analyses of reconstituted mice with sorted vWF^{+} HSCs revealed a similar platelet- and myeloid-biased blood production from both control and $NG2^{+}$ cell-depleted mice (**Figure 3F** and **S4B**). In addition, reconstitution of recipient mice with vWF^{-} HSCs was biased toward lymphoid lineage in both steady-state and $NG2^{+}$ cell-depleted mice (**Figure 3F-3H** and **S4B**). Furthermore, stable platelet-biased blood generation persisted for at least 16 weeks whether vWF^{+} HSCs were harvested from control or $NG2^{+}$ cell-depleted animals (**Figure 3F** and **S4B**). Whereas vWF^{-} HSCs from steady-state mice repopulated, as expected, only the vWF^{-} HSC compartment, some instances of vWF^{+} repopulation (25% of recipient mice) was observed from vWF^{-} HSCs harvested from $NG2^{+}$ cell-depleted BM (**Figure S4C**, third panel).

These results argue for the presence of spatially separate perivascular niches in the mouse BM that regulate functionally distinct subsets of lineage-biased quiescent HSCs. Phenotypic HSCs, like Nestin-GFP⁺/LepR⁺/CAR cells, are distributed throughout the BM (Acar et al., 2015; Kunisaki et al., 2013). However, the number of niche cells, whether defined by Nestin, LepR or CXCL12 expression, vastly outnumbers that of HSCs (by at least 20:1), underscoring the need for further stromal fractionation. We have previously suggested that the niche may be formed by the coupling of MSCs and HSCs (Mendez-Ferrer et al., 2010), a concept supported by the segregation of niche factor expression with MSC activity (Pinho et al., 2013). Further analyses fractionating and enriching MSC activity will be helpful to rule in or out this possibility. However, it is becoming clear that multiple cells in the microenvironment contribute to niche activity (Mendelson and Frenette, 2014). Among these are the arteriole-associated stromal cells which confer HSC quiescence as shown by the depletion of $NG2^{+}$ cells leading to HSC

redistribution and proliferation (Kunisaki et al., 2013). The role of arterioles as a specific microenvironment for HSC maintenance has been questioned by other studies which have used other markers to identify HSC *in situ* (Acar et al., 2015), but confirmed by others (Itkin et al., 2016). The present studies, using specific disruption of arterial and MK niches, further document their selective contributions in regulating the maintenance of distinct subsets of HSCs.

Vwf-driven GFP marking has allowed for the first time to evaluate the spatial distribution of specific lineage-biased HSC subsets *in situ*. Lineage bias in hematopoietic repopulation capacity has been retrospectively identified and defined by single HSC competitive transplantation experiments (Dykstra et al., 2007), but whether such lineage-biased HSCs occupy specific microenvironments or are uniformly distributed in the BM, remained unknown. Our studies show that myeloid-biased HSCs are enriched in MK niches whereas lymphoid-biased HSCs are enriched in arteriolar niches (**Figure 3I**). This contention is supported by their localization, and more importantly, by selective disruption of homeostasis using conditional depletion of these niches with genetically engineered models. These results support the notion that HSC niches are not uniform in the BM but rather formed by complex microenvironments with input from several cellular constituents. Interesting studies have suggested that HSC epigenetics may cell-autonomously regulate their fate. Serial transplantations of HSCs with defined hues reproduced the same complex pattern in lethally irradiated recipients, suggesting that the lineage contribution array may be intrinsically programmed by epigenetic memory (Yu et al., 2016). Our studies, however, show for the first time that a BM niche constituent (i.e. MK) may regulate HSC fate since MK deletion appears sufficient to reprogram vWf⁺ HSCs from myeloid-biased to balanced lineage contributions. As myeloid bias is a hallmark of HSC aging, understanding its molecular underpinnings may provide armamentarium for rejuvenation of aged

HSCs.

AUTHOR CONTRIBUTIONS

S.P. designed the study, performed the majority of the experiments and analysed data. T.M. helped with the whole-mount imaging experiments and analysed data. S.E.W.J. and C.N. provided the *Vwf-eGFP* mice and advised on experimental setup. P.S.F. supervised the study. S.P. and P.S.F. wrote the manuscript. All authors discussed the results and commented on the manuscript.

ACKNOWLEDGEMENTS

We would like to thank Colette Prophete and Paul Ciero for technical assistance, Lydia Tesfa and the Einstein Flow Cytometry Core Facility for expert cell sort assistance. S.P. was supported by a New York Stem Cell Foundation-Druckenmiller Fellowship; T.M. is supported by the Fondation ARC pour la Recherche sur le Cancer and by the Société Française d'Hématologie. This work was supported by the New York State Department of Health (NYSTEM Program), by the New York Stem Cell Foundation and by R01 grants from the National Institutes of Health (DK056638, HL116340, HL097819 to P.S.F.). The authors have no conflicting financial interests.

REFERENCES

- Acar, M., Kocherlakota, K.S., Murphy, M.M., Peyer, J.G., Oguro, H., Inra, C.N., Jaiyeola, C., Zhao, Z., Luby-Phelps, K., and Morrison, S.J. (2015). Deep imaging of bone marrow shows non-dividing stem cells are mainly perisinusoidal. *Nature* 526, 126-130.
- Asada, N., Kunisaki, Y., Pierce, H., Wang, Z., Fernandez, N.F., Birbrair, A., Ma'ayan, A., and Frenette, P.S. (2017). Differential cytokine contributions of perivascular haematopoietic stem cell niches. *Nat Cell Biol* 19, 214-223.
- Bruns, I., Lucas, D., Pinho, S., Ahmed, J., Lambert, M.P., Kunisaki, Y., Scheiermann, C., Schiff, L., Poncz, M., Bergman, A., *et al.* (2014). Megakaryocytes regulate hematopoietic stem cell quiescence through CXCL4 secretion. *Nature medicine* 20, 1315-1320.
- Chen, J.Y., Miyanishi, M., Wang, S.K., Yamazaki, S., Sinha, R., Kao, K.S., Seita, J., Sahoo, D., Nakauchi, H., and Weissman, I.L. (2016). Hoxb5 marks long-term haematopoietic stem cells and reveals a homogenous perivascular niche. *Nature* 530, 223-227.
- Copley, M.R., Beer, P.A., and Eaves, C.J. (2012). Hematopoietic stem cell heterogeneity takes center stage. *Cell Stem Cell* 10, 690-697.
- Dykstra, B., Kent, D., Bowie, M., McCaffrey, L., Hamilton, M., Lyons, K., Lee, S.J., Brinkman, R., and Eaves, C. (2007). Long-term propagation of distinct hematopoietic differentiation programs in vivo. *Cell Stem Cell* 1, 218-229.
- Gekas, C., and Graf, T. (2013). CD41 expression marks myeloid-biased adult hematopoietic stem cells and increases with age. *Blood* 121, 4463-4472.
- Itkin, T., Gur-Cohen, S., Spencer, J.A., Schajnovitz, A., Ramasamy, S.K., Kusumbe, A.P., Ledergor, G., Jung, Y., Milo, I., Poulos, M.G., *et al.* (2016). Distinct bone marrow blood vessels differentially regulate haematopoiesis. *Nature* 532, 323-328.
- Kiel, M.J., Yilmaz, O.H., Iwashita, T., Yilmaz, O.H., Terhorst, C., and Morrison, S.J. (2005). SLAM family receptors distinguish hematopoietic stem and progenitor cells and reveal endothelial niches for stem cells. *Cell* 121, 1109-1121.
- Kunisaki, Y., Bruns, I., Scheiermann, C., Ahmed, J., Pinho, S., Zhang, D., Mizoguchi, T., Wei, Q., Lucas, D., Ito, K., *et al.* (2013). Arteriolar niches maintain haematopoietic stem cell quiescence. *Nature* 502, 637-643.
- Kusumbe, A.P., Ramasamy, S.K., Itkin, T., Mae, M.A., Langen, U.H., Betsholtz, C., Lapidot, T., and Adams, R.H. (2016). Age-dependent modulation of vascular niches for haematopoietic stem cells. *Nature* 532, 380-384.
- Mendelson, A., and Frenette, P.S. (2014). Hematopoietic stem cell niche maintenance during homeostasis and regeneration. *Nature medicine* 20, 833-846.

- Mendez-Ferrer, S., Michurina, T.V., Ferraro, F., Mazloom, A.R., Macarthur, B.D., Lira, S.A., Scadden, D.T., Ma'ayan, A., Enikolopov, G.N., and Frenette, P.S. (2010). Mesenchymal and haematopoietic stem cells form a unique bone marrow niche. *Nature* *466*, 829-834.
- Muller-Sieburg, C.E., Sieburg, H.B., Bernitz, J.M., and Cattarossi, G. (2012). Stem cell heterogeneity: implications for aging and regenerative medicine. *Blood* *119*, 3900-3907.
- Nakamura-Ishizu, A., Takubo, K., Fujioka, M., and Suda, T. (2014). Megakaryocytes are essential for HSC quiescence through the production of thrombopoietin. *Biochem Biophys Res Commun* *454*, 353-357.
- Passequé, E., Wagers, A.J., Giuriato, S., Anderson, W.C., and Weissman, I.L. (2005). Global analysis of proliferation and cell cycle gene expression in the regulation of hematopoietic stem and progenitor cell fates. *The Journal of experimental medicine* *202*, 1599-1611.
- Pinho, S., Lacombe, J., Hanoun, M., Mizoguchi, T., Bruns, I., Kunisaki, Y., and Frenette, P.S. (2013). PDGFR α and CD51 mark human nestin⁺ sphere-forming mesenchymal stem cells capable of hematopoietic progenitor cell expansion. *The Journal of experimental medicine* *210*, 1351-1367.
- Sanjuan-Pla, A., Macaulay, I.C., Jensen, C.T., Woll, P.S., Luis, T.C., Mead, A., Moore, S., Carella, C., Matsuoka, S., Jones, T.B., *et al.* (2013). Platelet-biased stem cells reside at the apex of the haematopoietic stem-cell hierarchy. *Nature*.
- Shin, J.Y., Hu, W., Naramura, M., and Park, C.Y. (2014). High c-Kit expression identifies hematopoietic stem cells with impaired self-renewal and megakaryocytic bias. *The Journal of experimental medicine* *211*, 217-231.
- Yu, V.W., Yusuf, R.Z., Oki, T., Wu, J., Saez, B., Wang, X., Cook, C., Baryawno, N., Ziller, M.J., Lee, E., *et al.* (2016). Epigenetic Memory Underlies Cell-Autonomous Heterogeneous Behavior of Hematopoietic Stem Cells. *Cell* *167*, 1310-1322 e1317.
- Zhang, J., Niu, C., Ye, L., Huang, H., He, X., Tong, W.G., Ross, J., Haug, J., Johnson, T., Feng, J.Q., *et al.* (2003). Identification of the haematopoietic stem cell niche and control of the niche size. *Nature* *425*, 836-841.
- Zhao, M., Perry, J.M., Marshall, H., Venkatraman, A., Qian, P., He, X.C., Ahamed, J., and Li, L. (2014). Megakaryocytes maintain homeostatic quiescence and promote post-injury regeneration of hematopoietic stem cells. *Nature medicine* *20*, 1321-1326.

FIGURE LEGENDS

Figure 1. Platelet- and myeloid-biased vWF⁺ HSCs are exclusively associated with megakaryocytes in the mouse bone marrow

(A-B) Representative whole-mount images of *Vwf-eGFP* mouse sternal bone marrow (BM). The dashed outline in (A) denotes the bone–bone marrow border. (B) White arrowheads denote phenotypic Lineage[−] CD48[−] CD150⁺ vWF-eGFP⁺ HSCs; the open arrowhead denotes a phenotypic vWF-eGFP[−] HSC and the asterisk denote an arteriole. MK are distinguished by their size, morphology and CD150 and vWF expression. Vascular endothelial cells are stained intravenously with antibodies to CD31 and CD144. (C-D) Localization of vWF[−] and vWF⁺ HSCs relative to MK (C) and arterioles (D) in the mouse BM of *Vwf-eGFP* mice. (E) Percentage of vWF[−] and vWF⁺ HSCs located in direct contact (0 μm) with MK or arterioles. *P* values were determined by two-sample KS test (C and D) and unpaired Student's *t* tests (E). Error bars S.E.M.. See also Figures S1.

Figure 2. Platelet- and myeloid-biased vWF⁺ HSC proliferation and reconstitution potential are regulated by megakaryocytes

(A) Experimental design to test the effect of MK depletion on vWF⁺ and vWF[−] HSCs. (B) Representative FACS plots of the frequency of vWF⁺ and vWF[−] HSCs in the BM of control (*iDTR;Vwf-eGFP*) and *Cxcl4-cre;iDTR;Vwf-eGFP* mice, 7 days after diphtheria toxin (DT) treatment. (C) BM cellularity, (D) absolute number and (E) number of HSCs per femur in *iDTR;Vwf-eGFP* and *Cxcl4-cre;iDTR;Vwf-eGFP* mice normalized to control *iDTR*, 7 days after DT treatment. (F-H) Contribution of 100 LSK CD48[−] CD150⁺ vWF[−] and vWF⁺ HSCs from

iDTR;Vwf-eGFP and *Cxcl4-cre;iDTR;Vwf-eGFP* mice after MK depletion, to peripheral blood (F) platelets (16 weeks post-transplantation), (G) myeloid, B and T cells and (H) overall reconstitution at 16 weeks. * $P<0.05$, ** $P<0.01$, *** $P<0.001$; **** $P<0.0001$. Error bars S.E.M.. Unpaired Student's *t* tests (C, E, F and H). One-way ANOVA analyses followed by Tukey's multiple comparison tests were used for multiple group comparisons (D). See also Figures S2 and S3.

Figure 3. NG2⁺ arteriolar niche cells are critical regulators of the vWF[−] lymphoid-biased HSC quiescence and localization

(A) Experimental design to test the effect of NG2⁺ cells depletion on vWF⁺ and vWF[−] HSCs. (B) Representative FACS plots of the frequency of vWF⁺ and vWF[−] HSCs in the BM of control (*iDTR;Vwf-eGFP*) and *NG2-cre^{ERTM};iDTR;Vwf-eGFP* mice, 16 days after DT treatment. (C) BM cellularity, (D) absolute number and (E) number of HSCs per femur in *iDTR;Vwf-eGFP* and *Cxcl4-cre;iDTR;Vwf-eGFP* mice normalized to control *iDTR*, 16 days after DT treatment. (F-H) Contribution of 100 LSK CD48[−] CD150⁺ vWF[−] and vWF⁺ HSCs from *iDTR* and *Cxcl4-cre;iDTR* mice after MK depletion, to peripheral blood (F) platelets (16 weeks post-transplantation), (G) overall reconstitution and (H) myeloid, B and T cells at 16 weeks. (I) Summary of BM phenotypes of niche-structure-depleted mice in lineage-biased HSCs. * $P<0.05$, ** $P<0.01$, *** $P<0.001$. Error bars S.E.M.. Unpaired Student's *t* tests (C, E, F and G). One-way ANOVA analyses followed by Tukey's multiple comparison tests were used for multiple group comparisons (D). See also Figures S4.

Figure 4. Distribution of lineage-biased HSCs in the mouse BM after NG2⁺ cells depletion

Localization of phenotypic Lineage[−] CD48[−] CD150⁺ vWF-eGFP[−] (A, C) and vWF-eGFP⁺ (B, D) HSCs in the mouse BM relative to MK (A, B) and arterioles (C, D) in control (*iDTR;Vwf-eGFP*) and *NG2-cre^{ERTM};iDTR;Vwf-eGFP* mice, 16 days after DT treatment. *P* values were determined by two-sample KS test. Error bars S.E.M..

SUPPLEMENTAL FIGURE LEGENDS

Figure S1, related to Figure 1. vWF-eGFP⁺ cells constitute a small fraction of the LSK CD48[−] CD150⁺ HSC population in the mouse BM

(A) FACS gating strategy for the isolation of phenotypic Lineage (Lin)[−] Sca1⁺ c-Kit⁺ (LSK) CD48[−] CD150⁺ vWF-eGFP⁺ HSCs from the mouse BM of *Vwf-eGFP* mice. (B) 2D distribution of the distances between vWF-eGFP[−] (B) and vWF-eGFP⁺ (C) HSCs and MK or arterioles in the mouse sternal BM. Relative to **Figure 1C** and **1D**.

Figure S2, related to Figure 2. Distribution of lineage-biased HSCs in the mouse BM after MK depletion

Localization of phenotypic Lineage[−] CD48[−] CD150⁺ vWF-eGFP[−] (A,) and vWF-eGFP⁺ (B,) HSCs in the mouse BM relative to arterioles in control (*iDTR;Vwf-eGFP*) and *NG2-cre^{ERTM};iDTR;Vwf-eGFP* mice, 7 days after DT treatment. *P* values were determined by two-sample KS test. Error bars S.E.M..

Figure S3, related to Figure 2. Reconstitution potential of lineage-biased HSCs after MK depletion

(A) Experimental design of the competitive reconstitution assays used to determine the effect of MK depletion in the lineage potential of purified vWF^{-} and vWF^{+} HSCs. (B) Gating strategy for peripheral blood platelet reconstitution analysis in mice 16 weeks after competitive transplantation of CD45.2 vWF^{+} HSCs. (C) Quantification of tri-lineage (myeloid, B cell and T cell) and platelet engraftment in the peripheral blood of mice analyzed in **Figure 2F-H**. (D) Representative BM FACS plots showing donor HSCs contribution to recipient CD45.2⁺ LSK CD48⁻ CD150⁺ $vWF-eGFP^{-}$ or $vWF-eGFP^{+}$ HSC compartment at 16 weeks from the mice analyzed in **Figure 2F-H**. * $P < 0.05$, ** $P < 0.01$. Error bars S.E.M.. Unpaired Student's *t* tests (C).

Figure S4, related to Figure 3. Reconstitution potential of lineage-biased HSCs after NG2+ cells depletion

(A) Experimental design of the competitive reconstitution assays used to determine the effect of NG2⁺ cells depletion in the lineage potential of purified vWF^{-} and vWF^{+} HSCs. (B) Quantification of trilineage (myeloid, B cell and T cell) and platelet engraftment in the peripheral blood of mice analyzed in **Figure 3F-H**. (C) Representative BM FACS plots showing donor HSCs contribution to recipient CD45.2⁺ LSK CD48⁻ CD150⁺ $vWF-eGFP^{-}$ or $vWF-eGFP^{+}$ HSC compartment at 16 weeks from the mice analyzed in **Figure 3F-H**. * $P < 0.05$, *** $P < 0.001$. Error bars S.E.M.. Unpaired Student's *t* tests (B).

METHODS

Mice

C57BL/6-Tg(Cxcl4-iCre)Q3Rsko/J (*Cxcl4*-cre), B6.Cg-Tg(Cspg4-cre/Esr1*)BAkik/J (*NG2*-cre^{ERTM}) and C57BL/6-*Gt(ROSA)26Sor^{tm1(HBEGF)Awai}*/J (*iDTR*) mice were purchased from the Jackson Laboratory. *Vwf-EGFP* transgenic mice were previously described (Sanjuan-Pla et al., 2013). C57BL/6 (CD45.2) and B16-Ly5.1 (CD45.1) mice were purchased from the National Cancer Institute or the Jackson laboratory (B6.SJL-*Ptprc^a Pepc^b*/BoyJ). Unless indicated otherwise, 8–12-week-old male and female mice were used. No randomization or blinding was used to allocate experimental groups. The Animal Care and Use Committees of Albert Einstein College of Medicine approved all experimental procedures.

In vivo treatments

For DT-mediated MK depletion, 250 ng of DT (Sigma) was injected intraperitoneally (i.p.) every 24 hours over 7 days. Mice were subjected to HSC analyses on the day of the last injection. For induction of *NG2*-cre^{ERTM}-mediated recombination mice were injected i.p. with 2 mg tamoxifen (Sigma) dissolved in corn oil (Sigma) once a day during 5 consecutive days. For DT-mediated *NG2*⁺ cells depletion, 2 days after the last tamoxifen injection, mice were injected i.p. with 250 ng of DT (Sigma) once a day during 2 days.

Whole-mount immunofluorescence imaging

Whole-mount tissue preparation, HSC immunofluorescence staining and imaging of the sternum were performed as described previously (Bruns et al., 2014; Kunisaki et al., 2013).

Antibodies

The following antibodies were used in this study: anti-Ly6A/E (D7), anti-CD117 (2B8), anti-CD48 (HM48-1), anti-CD41 (MWReg30), anti-CD45.2 (104), anti-CD45.1 (A20), anti-CD4 (GK1.5), anti-CD8 (53-6.7), anti-B220 (RA3-6B2), anti-CD11b (M1/70), anti-CD31 (MEC13.3), anti-CD144 (BV13), anti-CD31 (MEC13.3) were all from eBioscience. Anti-CD150 (TC15-12F12.2), and anti-Ter119 (TER-119) were from Biolegend. Anti-Lineage panel cocktail (TER-119, RB6-8C5, RA3-6B2, M1/70, 145-2C11 at 1:50 dilution) was from BD Biosciences. Unless otherwise specified, all antibodies were used at a 1:100 dilution.

Flow cytometry and cell sorting

Flow cytometric analyses were carried out in single-cell suspensions of nucleated cells enriched from the peripheral blood or flushed bone marrow using an LSRII flow cytometer (BD Biosciences). Cell sorting experiments were performed using a FACS Aria Cell Sorter (BD Biosciences). Dead cells and debris were excluded by FSC, SSC and DAPI (4',6-diamino-2-phenylindole) staining profiles. Data were analysed with FlowJo (Tree Star) or FACS Diva 6.1 software (BD Biosciences).

Bone marrow transplantation

Competitive repopulation assays were performed using the CD45.1/CD45.2 congenic system. Recipient mice were lethally irradiated (12 Gy, two split doses) in a Cesium Mark 1 irradiator (JL Shepherd & Associates). 100 vWF⁻ or vWF⁺ CD45.2⁺ HSCs (defined as LSK CD48⁻ CD150⁺) were isolated from the bone marrow of *Cxcl4-cre; iDTR; Vwf-eGFP* or from *NG2-*

cre^{ERTM};iDTR;Vwf-eGFP and respective littermate control *iDTR;Vwf-eGFP* mice. Sorted HSCs were intravenously transplanted together with 0.25×10^6 competitor CD45.1⁺ total BMNCs. CD45.1/CD45.2 chimerism of recipient blood was analysed up to 4 months after transplantation using FACS. Blood was harvested by submandibular route and collected in polypropylene tubes containing EDTA. Mice showing more than 1% donor reconstitution in the myeloid (CD11b⁺), B-cell (B220⁺) and T-cell (CD4⁺ CD8⁺) lineages after 16 weeks were considered engrafted. The percentage of platelet chimerism was calculated as previously described (Sanjuan-Pla et al., 2013) briefly whole peripheral blood was centrifuged for 10 min at 100g and platelet-containing supernatant was stained. Plasma-derived platelets were identified based on scatter properties, absence of Ter119 and CD41, CD150 and eGFP expression.

Statistics

All data are represented as mean \pm S.E.M.. Comparisons between two samples were done using the unpaired Student's *t* tests. One-way ANOVA analyses followed by Tukey's multiple comparison tests were used for multiple group comparisons. Two-sample Kolmogorov–Smirnov tests were used for comparisons of distribution patterns. Statistical analyses were performed with GraphPad Prism. **P* < 0.05, ***P* < 0.01, ****P* < 0.001, *****P* < 0.0001.

Figure 1

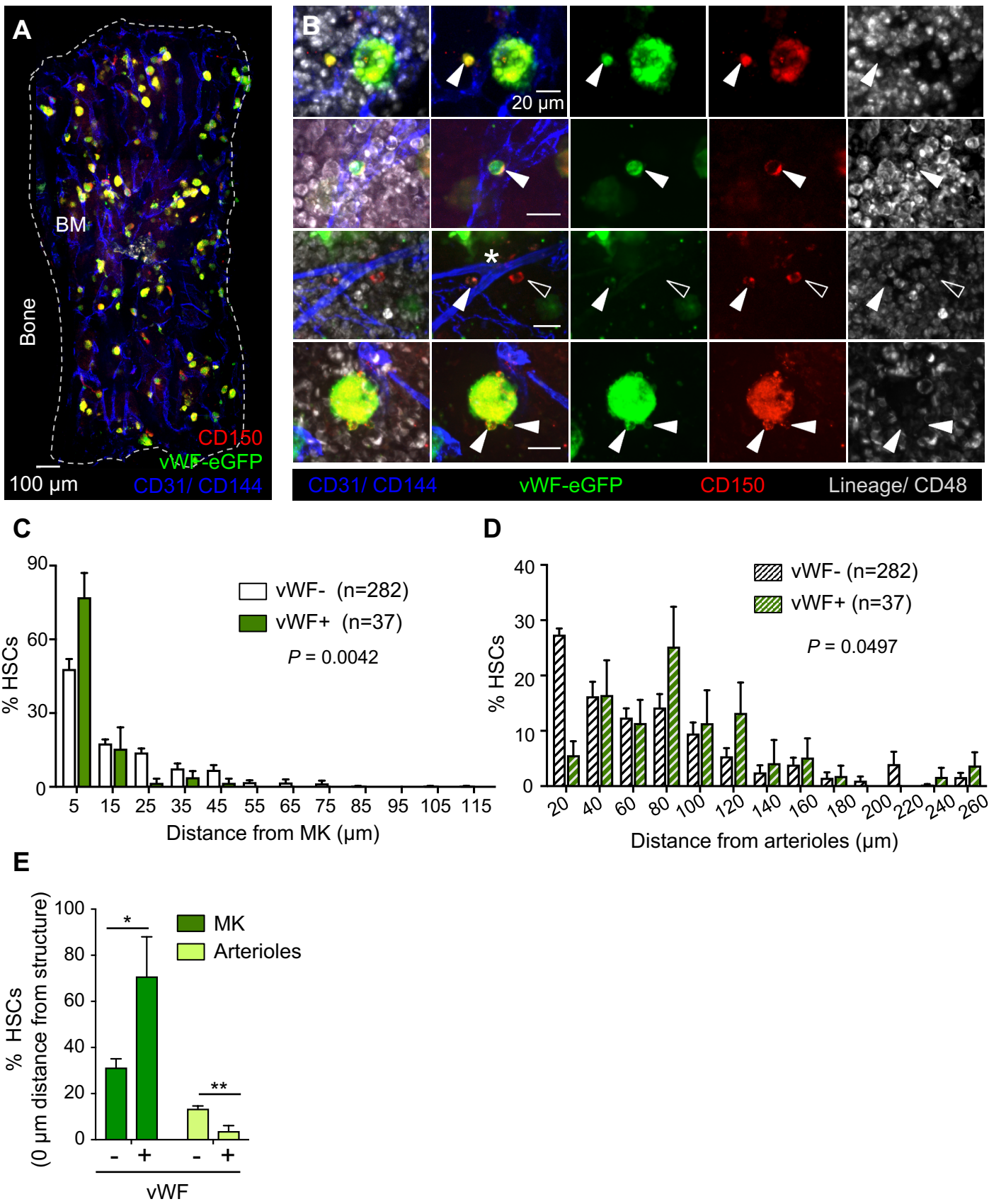


Figure 2

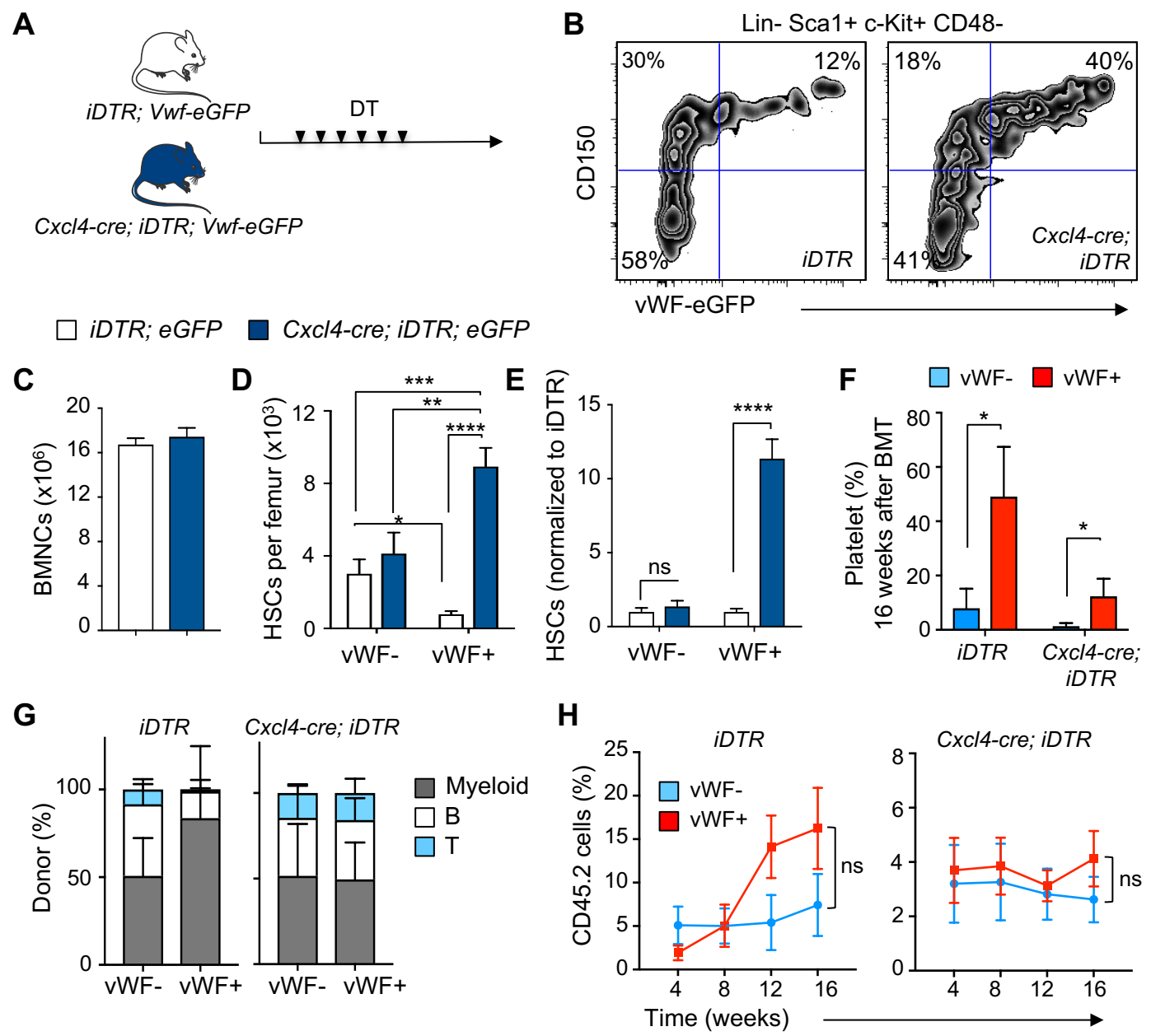
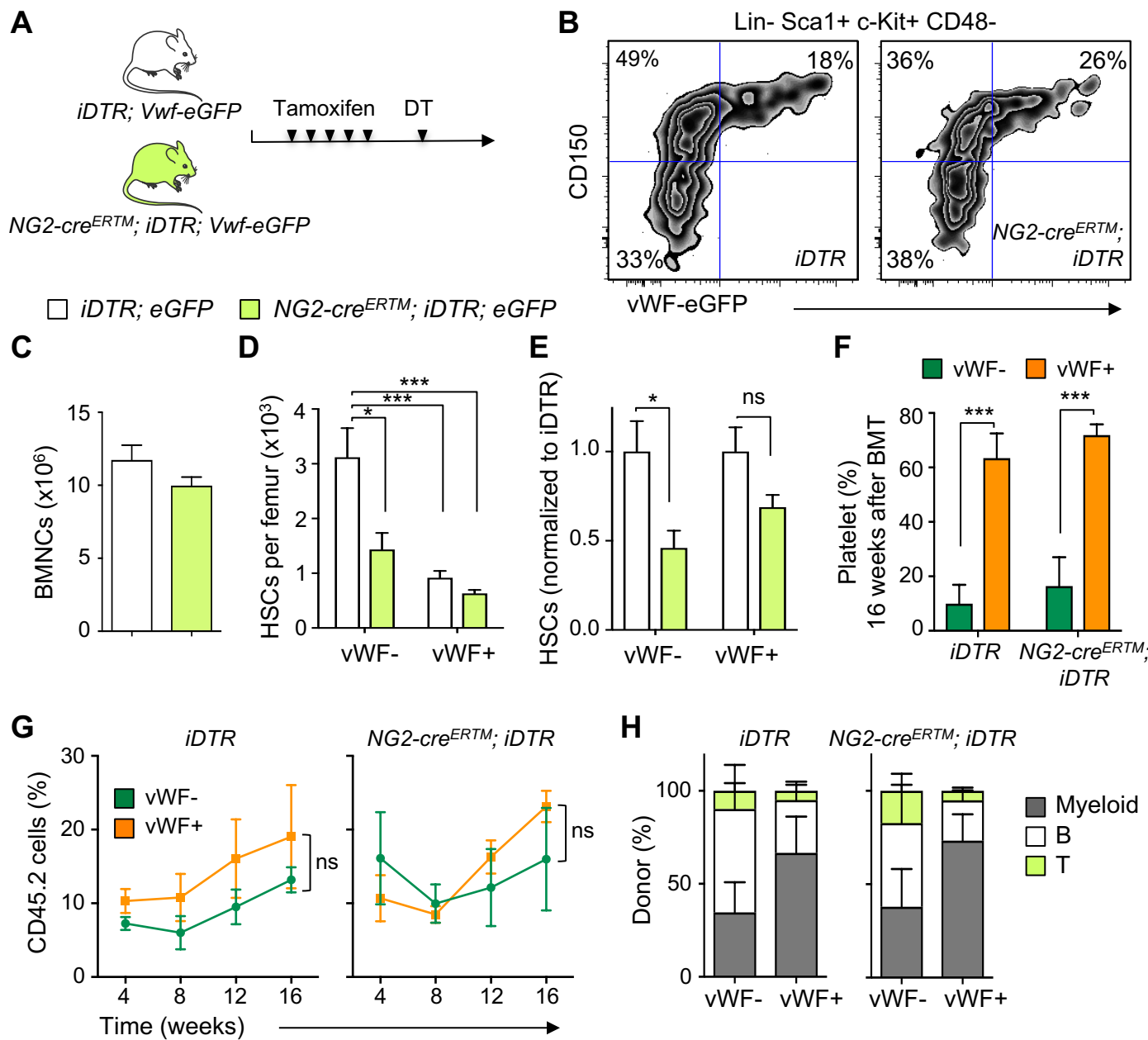


Figure 3

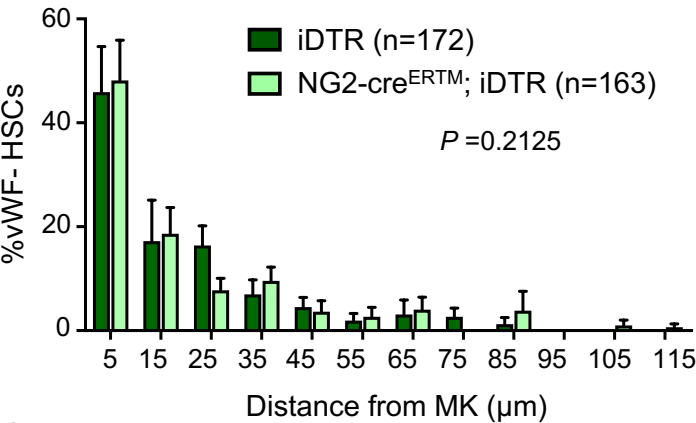


I

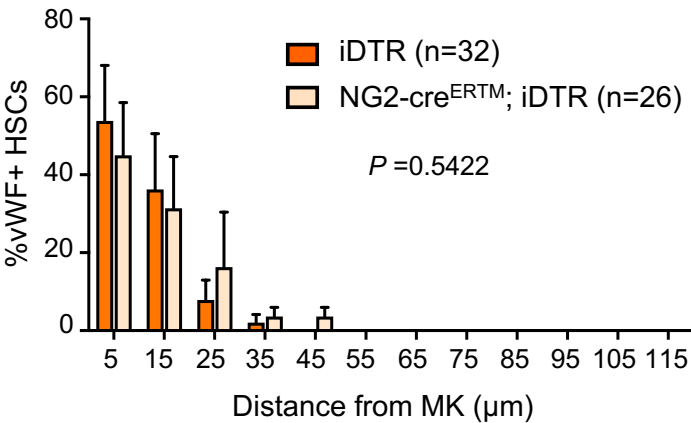
Genetic model	HSC cell number		HSC preferred niche association			
			Megakaryocytic		Arteriolar	
	vWF-	vWF+	vWF-	vWF+	vWF-	vWF+
<i>iDTR</i> (control)			✓	✓	✓	✗
<i>Cxcl4-cre; iDTR</i>	↑	↑↑↑↑			✓	✗
<i>NG2-cre^{ERTM}; iDTR</i>	↓↓↓	↓	✓	✓	✗	✗

Figure 4

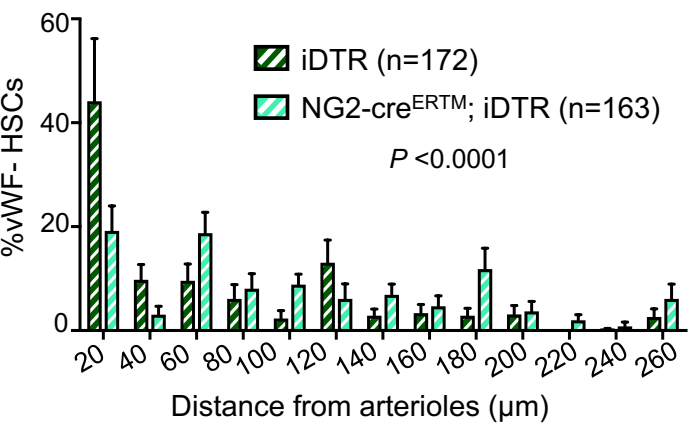
A



B



C



D

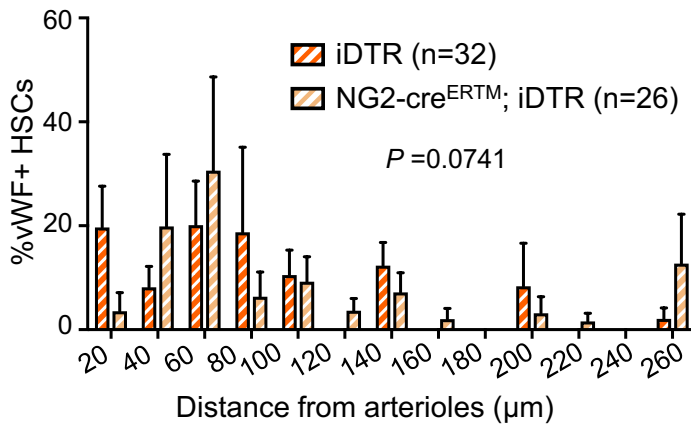


Figure S1. Related to Figure 1

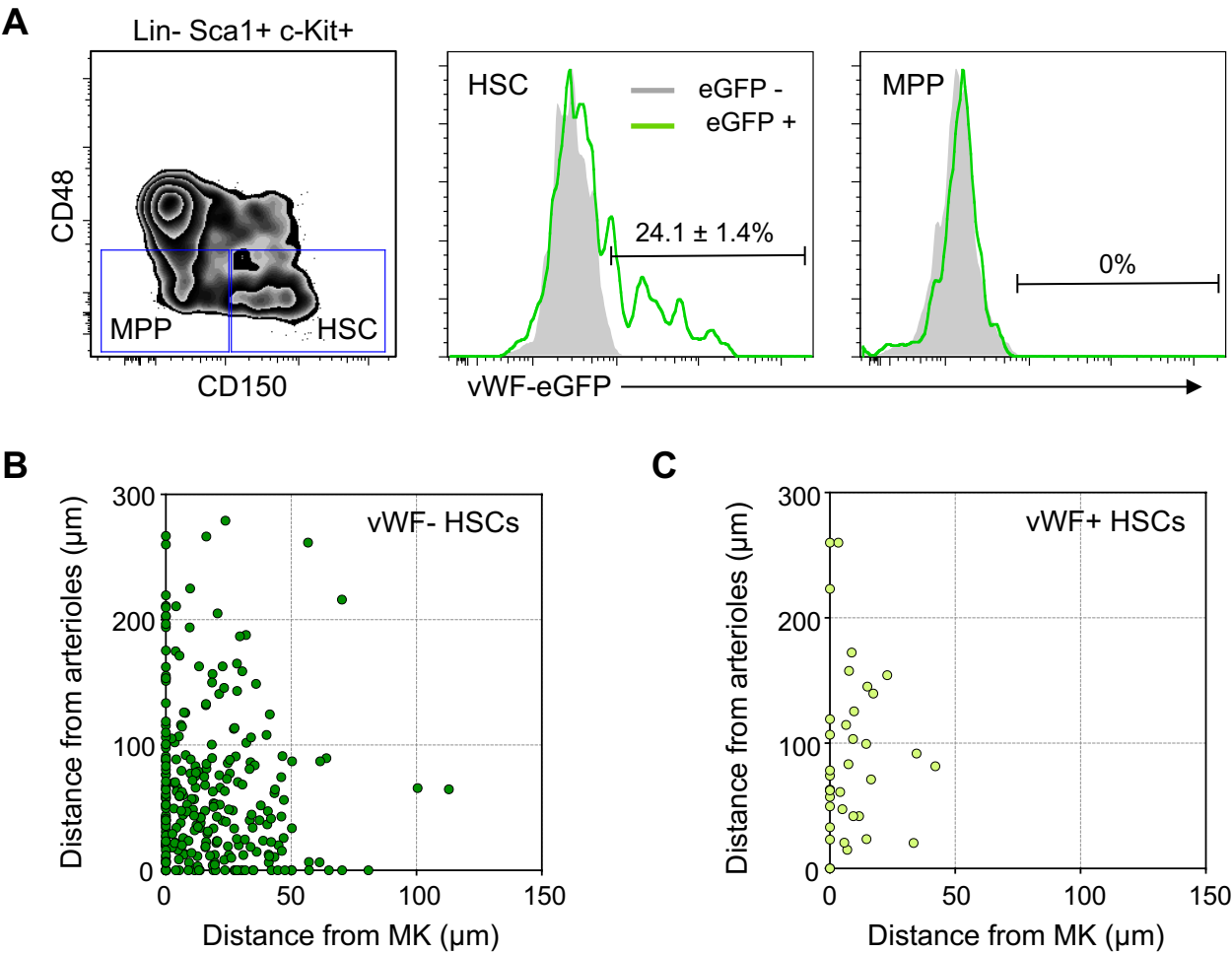


Figure S2. Related to Figure 2

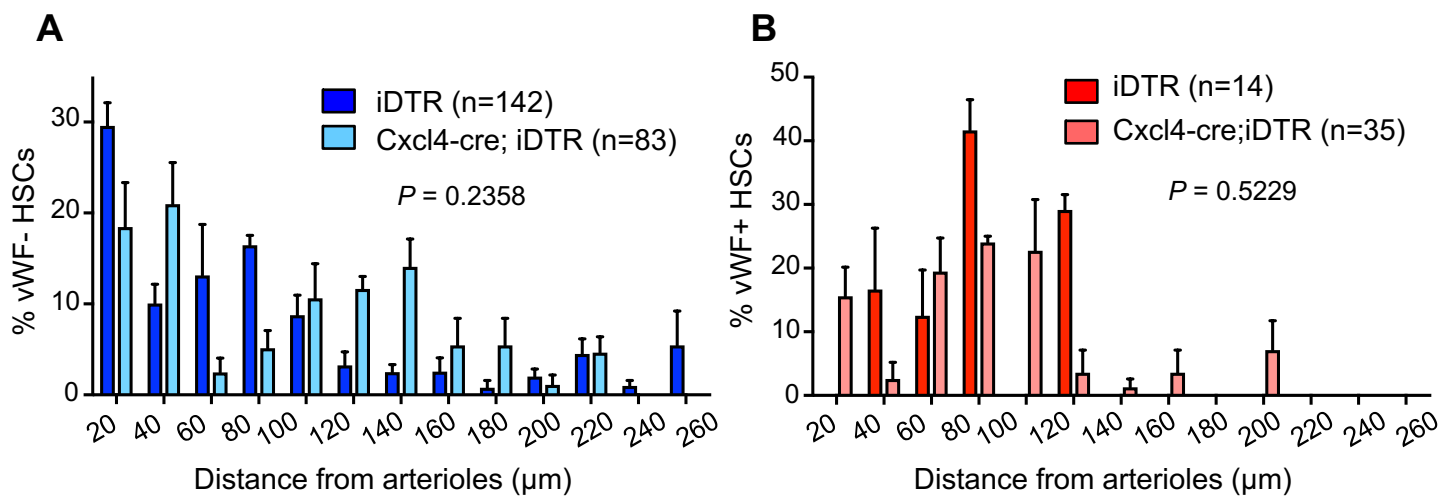
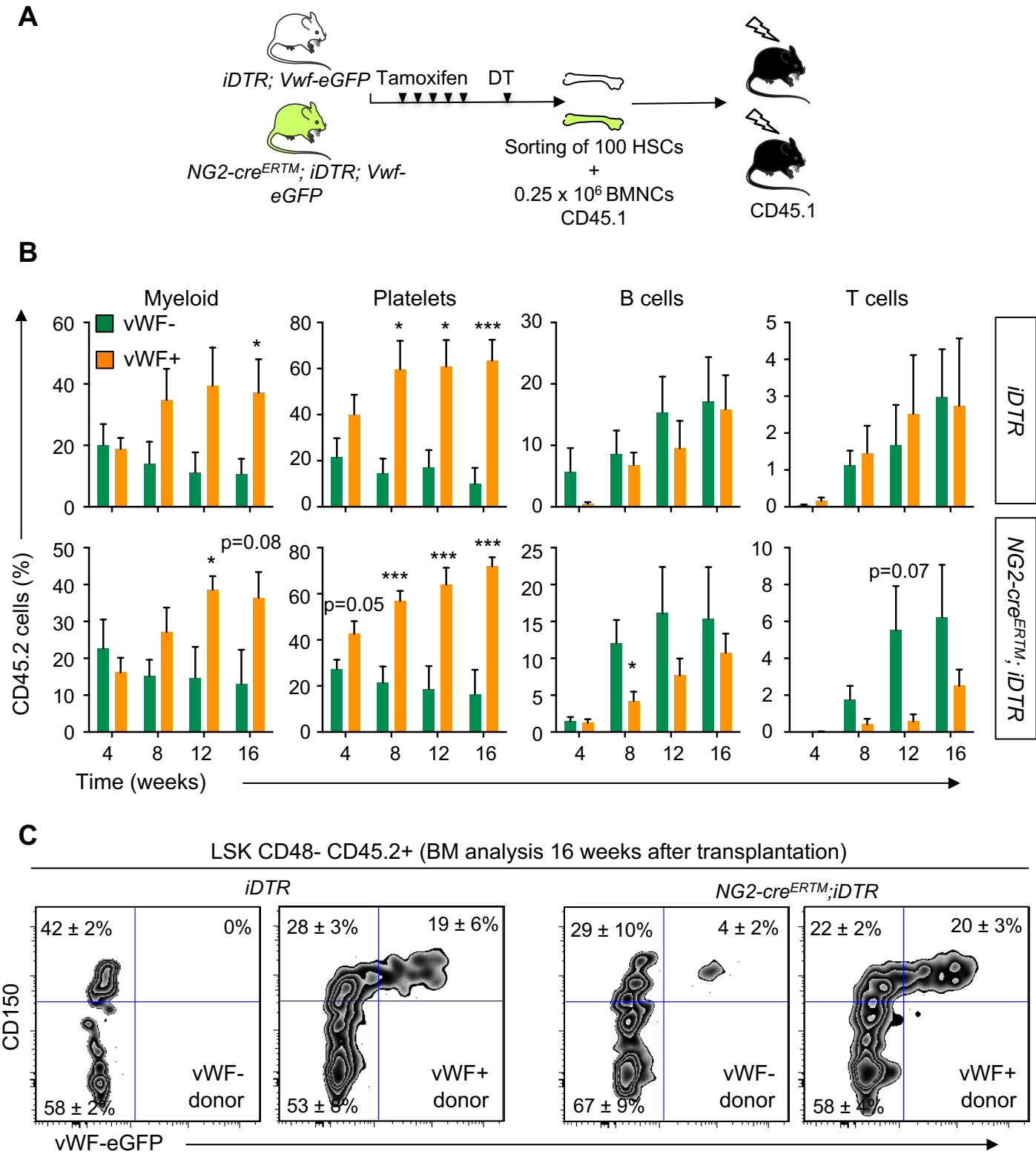


Figure S4. Related to Figure 3



Graphical abstract

